Dynamic trajectory control of gliders

Rui DILãO and João FONSECA

Institut des Hautes Études Scientifiques
35, route de Chartres
91440 – Bures-sur-Yvette (France)

Avril 2013

IHES/M/13/09

Dynamic trajectory control of gliders

Rui Dilão[1,2] and João Fonseca[1]

Abstract A new dynamic control algorithm in order to direct the trajectory of a glider to a pre-assigned target point is proposed. The algorithm runs iteratively and the approach to the target point is self-correcting. The algorithm is applicable to any non-powered lift-enabled vehicle (glider) travelling in planetary atmospheres. As a proof of concept, we have applied the new algorithm to the command and control of the trajectory of the Space Shuttle during the Terminal Area Energy Management (TAEM) phase.

1 Introduction

Space vehicles travel at extreme conditions of speed and acceleration that typically do not allow for a "man-in-the loop" approach, forcing, at least partially, automation of the flight controls. Thus, automated guidance and control systems are a critical component for any re-usable space flight vehicle.

For example, the implementation of control mechanisms for atmosphere re-entry and automatic landing systems used in the Space Shutle focused either on pre-programmed manoeuvres following a nominal pre-computed trajectory, or hopping across different nominal trajectories whenever the vehicle deviates from an initially selected trajectory, [11] and [4].

A typical return flight from space has three main phases:

1) Atmospheric re-entry phase: In this initial re-entry phase the transition from spacecraft to aircraft flight mode occurs. The typical altitudes for this phase are in the range 120-40 km.

Nonlinear Dynamics Group, Instituto Superior Técnico, Av. Rovisco Pais, 1049-001 Lisbon, Portugal rui@sd.ist.utl.pt, jlpfonseca@gmail.com · Institut des Hautes Études Scientifiques, 35, route de Chartres, 91440 Bures-sur-Yvette, France.

2) Glide to the landing site phase, usually referred as Terminal Area Energy Management (TAEM), occurring in the altitude range 40-3 km.
3) Final approach and landing phase, occurring in the altitude range 3-0 km.

While in the atmosphere re-entry phase, the biggest priority is to ensure that the structural constraints of the vehicle are not exceeded; during the TAEM phase, the biggest priority is to ensure that the vehicle reaches the Heading Alignment Circle (HAC) where preparation for landing is initiated.

On a typical mission, the TAEM phase begins at the altitude of $25,000-40,000$ m at a speed around $2-6$ M (Mach), and finishes at the HAC at the altitude of $1,500-3,000$ m, with a speed of the order of 0.20 M.

In this paper, we propose a new dynamic control algorithm in order to redirect the trajectory of gliders to a pre-assigned target point. This algorithm runs iteratively enabling a self-correcting approach to the HAC and is applicable to any non-powered lift-enabled vehicle (glider) travelling in planetary atmospheres.

This paper is organised as follows. In section 2, we present the equations of motion of a glider and we discuss the approximations we use to define the controllability conditions. In section 3, we briefly discuss the phenomenology of aircraft gliding motion, instrumental for the design of a dynamic control strategy. In section 4, we derive the dynamic control algorithm, and in section 5 we present realistic simulations for the Space Shuttle TAEM guidance and control. Finally, in section 6 we discuss the main conclusions of the paper.

2 Gliding motion

We consider that aircraft gliding motion in a planetary atmosphere is well described by a point mass vehicle model under the influence of a gravity field, [3], [5], [9] and [2]. In this case, the equations of motion of a gliding aircraft (no thrust forces) are,

$$\begin{cases} m\dot{V} = -mg(z)\sin\gamma - D(\alpha,Ma) \\ mV\dot{\gamma} = -mg(z)\cos\gamma + L(\alpha,Ma)\cos\mu \\ mV\dot{\chi}\cos\gamma = L\sin\mu \end{cases}, \begin{cases} \dot{x} = V\cos\chi\cos\gamma \\ \dot{y} = V\sin\chi\cos\gamma \\ \dot{z} = V\sin\gamma \end{cases} \tag{1}$$

where m is the aircraft mass, $V=\sqrt{V_x^2+V_y^2+V_z^2}$ is the aircraft speed, γ is the flight path angle as defined in figures 1 and 2, μ is the bank angle as defined in figure 2c), $D(\alpha,Ma)$ and $L(\alpha,Ma)$ are the drag and lift forces induced by the atmosphere, α is the angle of attack and Ma is the Mach number. In general, the Mach number Ma is a function of V and z. The function $g(z)=g_0(R_E/(R_E+z))^2$ is the gravity acceleration, $g_0=9.80665$ m/s^2 is the Earth standard gravitational acceleration constant and $R_E=6.371\times10^6$ m is the Earth (or planetary) mean radius.

In the local reference frame of the aircraft, figure 1, $V\in(0,\infty)$, $\gamma\in[-\pi/2,\pi/2]$ and $\chi\in[0,2\pi]$. The bank angle μ is defined in the interval $[-\pi/2,\pi/2]$. In this reference frame, positive values of μ correspond to left turns and negative values of

μ correspond to right turns. As usual, $(x,y,z) \in \mathbb{R}^3$ and $(\dot{x},\dot{y},\dot{z}) \in \mathbb{R}^3$. In the system of equations (1), α and μ can be seen as input parameters.

To define the local system of coordinates, we have used a flat-Earth approach. As we want to analyse the motion of gliders during the TAEM phase, the height at which the TAEM phase starts is very small when compared to the Earth radius, justifying our analysis. However, this approach can be further refined by using an ellipsoidal coordinate system adequate to Earths shape, such as the WGS-84 coordinate system.

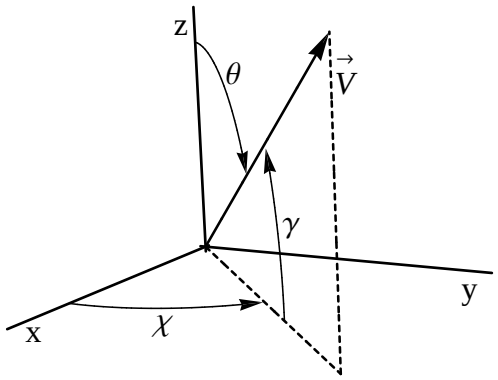

Fig. 1 Local coordinate system for the point mass glider model. The origin of coordinates is located at the centre of mass of the aircraft, and the vector **V** is the velocity vector not necessarily collinear with the aircraft longitudinal axis.

In figure 2a)-b), we show the angle of attack α defined as the angle between the longitudinal reference line of the aircraft and the vector velocity of the aircraft. In airplanes, the angle of attack is always a positive angle. While in most aircrafts attack angles are always smaller than 15^o, the Space Shuttle is capable of attack angles up to 45^o, [8] and [7]. In figure 2c), we show the bank angle, defining the inclination of the aircraft in the plane containing the velocity vector.

The drag and lift forces in the system of equations (1) are given by,

$$\begin{aligned} D(\alpha,Ma) &= \bar{q}SC_D(\alpha,Ma) = \tfrac{1}{2}\rho(z)V^2SC_D(\alpha,Ma) \\ L(\alpha,Ma) &= \bar{q}SC_L(\alpha,Ma) = \tfrac{1}{2}\rho(z)V^2SC_L(\alpha,Ma) \end{aligned} \tag{2}$$

where $\bar{q} = \rho(z)V^2/2$ is the dynamic pressure, S is the wing area of the aircraft, $\rho(z)$ is the atmosphere density as a function of altitude (Appendix) and Ma is the Mach number. For each specific aircraft, the functions $C_D(\alpha,Ma)$ and $C_L(\alpha,Ma)$ are the aerodynamic drag and lift coefficients determined in wind tunnel experiments.

Introducing the expressions (2) into equations (1), we obtain the final form for the equations of motion of a glider,

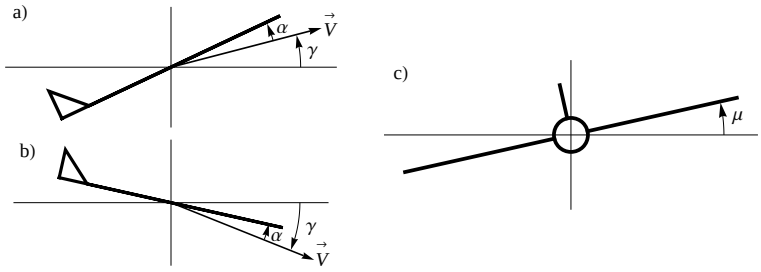

Fig. 2 In a) and b), we show the flight path angle γ and the angle of attack α of an aircraft. In c) we show the bank angle μ, measuring the inclination of the aircraft in the plane containing the velocity vector and the horizontal direction. The flight path angle γ depends on the angle of attack, on the aerodynamic coefficients of the aircraft and on the Mach number. The control of a glider is done by the manipulation of the angles of attack and bank.

$$\begin{cases} \dot{V} = -g(z)\sin\gamma - \left(\dfrac{1}{2m}\rho(z)SC_D(\alpha,Ma)\right)V^2 \\ \dot{\gamma} = -\dfrac{g(z)}{V}\cos\gamma + \left(\dfrac{1}{2m}\rho(z)SC_L(\alpha,Ma)\right)V\cos\mu \\ \dot{\chi} = \left(\dfrac{1}{2m}\rho SC_L\right)V\dfrac{\sin\mu}{\cos\gamma} \end{cases}, \begin{cases} \dot{x} = V\cos\chi\cos\gamma \\ \dot{y} = V\sin\chi\cos\gamma \\ \dot{z} = V\sin\gamma. \end{cases} \quad (3)$$

where $\rho(z)$ is calculated in the Appendix.

The aircraft gliding trajectory is described by the system of equations (3), enabling a simple geometric solution of the gliding aircraft control problem.

When a glider is falling under a gravity field it converges to a steady state motion with a constant velocity and constant flight path angle given by, [1],

$$\begin{aligned} V^* &= \sqrt{\frac{2mg}{\rho S}}\frac{1}{(C_D^2 + C_L^2\cos^2\mu)^{1/4}} \\ \gamma^* &= -\arctan\frac{C_D}{C_L\cos\mu} \end{aligned} . \quad (4)$$

The geometry of the solutions of equation (3) in phase space are analysed in detail in [1].

3 Phenomenology of Space Shuttle gliding motion

Using wind tunnel data for the operational range of aircrafts during the TAEM phase, we have done fits for the aerodynamic drag and lift coefficients C_D and C_L of the Space Shuttle and these are well described by the parameterised functions,

$$\begin{aligned} C_L(\alpha,Ma) &= (a_1 + a_2\alpha + a_3\alpha^2)K(Ma)^{b_1+\alpha b_2} \\ C_D(\alpha,Ma) &= (0.01 + f_1 Ma^{f_2} + d_3\alpha^2)K(Ma)^{e_1+\alpha e_2} \end{aligned} \tag{5}$$

where,

$$K(Ma) = \frac{1}{2}\left(1 + \sqrt{\left|1 - \left(\frac{Ma}{M_c}\right)^2\right|}\right) \tag{6}$$

is a simplification of the Van Karman functions expanded to supersonic regimes, [8]. In table 1, we show, for the Space Shuttle, the parameter estimation of expressions (5) and (6) with wind tunnel data.

Parameter	Estimated	Standard error	t-statistics	P-value
a_1	-0.053	0.009	-6.15	9.8×10^{-8}
a_2	2.73	0.06	43.0	1.8×10^{-43}
a_3	-1.55	0.09	-18.0	2.0×10^{-24}
b_1	-1.01	0.09	-11.3	7.4×10^{-16}
b_2	1.1	0.1	8.7	7.6×10^{-12}
d_3	1.79	0.02	99.0	1.1×10^{-63}
e_1	-1.4	0.1	-12.6	1.2×10^{-17}
e_2	1.5	0.1	11.3	5.8×10^{-16}
f_1	0.028	0.004	6.46	2.9×10^{-8}
f_2	1.4	0.2	8.57	1.0×10^{-11}
M_c	1.25	0.03	49.6	1.0×10^{-46}

Table 1 Parameters of the aerodynamic drag and lift coefficients (5) for the Space Shuttle, estimated from wind tunnel data, [6]. The significance of the fits have been determined with a chi-squared test. The large values of the absolute value of the t-statistics measures the likelihood of the parameters in the fits. The low values of the p-values mean that the fits are highly significant and the probability of finding a value outside the fitted ones are in the range $10^{-8} - 10^{-63}$.

Introducing the expressions of $C_L(\alpha,Ma)$ and $C_D(\alpha,Ma)$ into (4), changing the angle of attack α and the bank angle μ leads to changes in the local steady states of the glider (see (4)), enabling a guided control of the direction of motion and of the glider speed.

To control the aerodynamic behaviour of an aircraft, two main parameters are under the control of the aircraft commands: i) the bank angle μ, and ii) the attack angle α.

The bank angle μ determines the inclination of the aircraft and is used for turn manoeuvres, figure 2c).

The no-lift angle α_{nL}, the max-glide angle α_{maxgl} and stall angle α_{stall} are particular limits of the angle of attack of an aircraft, figure 2a) and 3.

In figure 3, we show, for several values of the Mach number, the behaviour of the ratio L/D, as a function of the angle of attack α for the Space Shuttle. All the curves intersect at the no-lift angle α_{nL}. The no-lift angle α_{nL} is the angle for which L/D is zero due the absence of the lift force and is independent of the speed. The max-glide angle α_{maxgl} is the angle that maximises the ratio L/D, and is dependent on

the Mach number. The stall angle α_{stall} is the angle at which lift dependency looses linearity and lift peaks before beginning to decrease. The stall angle is independent of the Mach number.

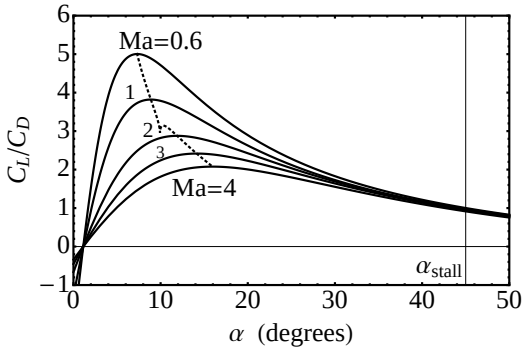

Fig. 3 Ratio L/D, as a function of the angle of attach α, for the Space Shuttle at different Mach numbers, calculated from (5)-(6) and table 1. The no-lift parameter is $\alpha_{nL} = 1.5^o$, the stall angle is $\alpha_{stall} = 45^o$ and α_{maxgl} is given by (7). The Space Shuttle is a glider and thus can only move across its L/D curve. For higher speeds this curve will become increasingly flat and the max-glide angle α_{maxgl} will move further to the right reaching saturation.

With the functions (5)-(6), we have approximated the max-glide angle α_{maxgl} as a function of Mach number. For the case of the Space Shuttle, we have obtained,

$$\alpha_{maxgl} = \begin{cases} 0.0906 + 0.0573Ma + 0.0071Ma^2 & (Ma \leq 1.25) \\ 0.1070 + 0.0577Ma - 0.0037Ma^2 & (1.25 < Ma < 5) \end{cases} \tag{7}$$

determined with a correlation coefficient of $r^2 = 0.999$. The Mach number is defined by $Ma = V/V_{sound}$ where the sound speed is calculated with,

$$V_{sound} = \sqrt{\gamma T(z) R_s} \tag{8}$$

and $T(z)$ is given in table 2 in the Appendix. $\gamma = 1.4$ is the diatomic gas constant and $R_s = 287.04$ J/(kg K).

4 Dynamic trajectory control of gliders

A glider is not always in an equilibrium state but naturally converges to it given enough time. Our algorithm will take advantage of this behaviour by determining the equilibrium conditions needed to reach the target, imposing them on the system and letting it evolve in time.

To define the control problem, we consider the initial condition,

$$(x_0, y_0, z_0, V_0, \gamma_0, \chi_0)$$

defining the initial coordinates of the TAEM phase. Let,

$$(x_f, y_f, z_f)$$

be the space coordinates of the target, which coincide with the central point in the HAC region. We consider that the target point is only defined by the spatial coordinates of the HAC, and the direction of the velocity vector is arbitrary. In fact, this is possible at low altitudes (3 km) because the atmosphere is dense enough to allow the glider to preform turns in short distances and the vehicle is always travelling near the equilibrium speed.

The intermediate coordinates of the glider path are,

$$(x_i, y_i, z_i, V_i, \gamma_i, \chi_i)$$

where $i = 0, 1, \ldots, f$. These intermediate coordinates are evaluated at time intervals T_{con}.

In the configuration space (x, y, z), we define the direction vector from the current position of the glider to the target point as,

$$\mathbf{P}_i = (x_f - x_i, y_f - y_i, z_f - z_i)\,. \tag{9}$$

In order to direct the aircraft to the target, we control the attack and bank angles separately.

In the **attack angle heading control**, we analyse the glider trajectory in the three dimensional ambient space (x, y, z), and we command the glider trajectory path angle by controlling the angle of attack α.

In the **bank angle heading control**, the control procedures will be done in the (x, y) plane by adjusting the bank angle μ.

At the step number i of the dynamic control process, the initial conditions are $(x_i, y_i, z_i, V_i, \gamma_i, \chi_i)$. At this stage, the angle of attack and bank angle are α_i and μ_i. Then, we calculate the new values of the glider control parameters α_{i+1} and μ_{i+1} by the two procedures described below. With these new values for α and μ , the aircraft will follow a new trajectory during the time interval T_{con}, figure 4.

This control process is done sequentially in time, until the glider reaches de HAC region. In practical terms, the control mechanisms stops when the distance from the spacecraft to the centre of the HAC point attains a minimum.

We analyse now in detail the two control and command procedures for α and μ.

Attack angle heading control:

The attack angle heading command and control was designed so that the vehicle is always re-orienting vertically to the HAC point through a straight line path.

The tangent of the angle between the $x - y$ projection and the z component of the direction vector P_i to the target point is computed at each iteration, and we obtain,

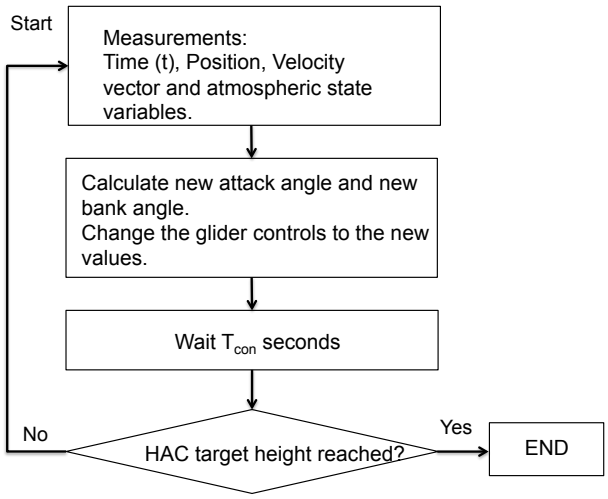

Fig. 4 Block diagram for the controller algorithm.

$$G_{i+1} = \frac{(z_f - z_i)}{\sqrt{(x_f - x_i)^2 + (y_f - y_i)^2}}$$

where (x_i, y_i, z_i) is the current position of the glider. At this position, the glider has flight path γ_i. Then, to direct the motion of the glider to the target with a steady flight path, by (4), we must have,

$$G_{i+1} = \tan\gamma = -\frac{1}{C_L/C_D \cos\mu_{i+1}}\,. \tag{10}$$

Assuming that it is possible to direct the motion to the target using a null bank angle, $\mu_{i+1} = 0$, we solve equation (10) in order to the ratio C_L/C_D, and we obtain the solution c_{i+1}. Then:

a) If c_{i+1} is bigger than $C_L(\alpha_{maxgl}, Ma_i)/C_D(\alpha_{maxgl}, Ma_i)$, the target cannot be reached in a straight-line and the max-glide attack angle will be selected, $\alpha_{i+1} = \alpha_{maxgl}$. The curve of C_L/C_D as a function of α and of the Mach number Ma is given by (5) and (6), and α_{maxgl} is calculated from (7) and (8).
b) If c_{i+1} is smaller than $C_L(\alpha_{stall}, Ma_i)/C_D(\alpha_{stall}, Ma_i)$, the target cannot be reached in a straight-line and the stall angle will be selected, $\alpha_{i+1} = \alpha_{stall}$.
c) Otherwise, the attack angle α_{i+1} is computed by solving the equation $C_L(\alpha, Ma_i)/C_D(\alpha, Ma_i) = c_{i+1}$.

At this stage, we have chosen a new attack angle α_{i+1}. With this new attack angle, we re-orient dynamically and vertically the aircraft trajectory to the target.

Bank angle heading control:

The bank angle heading control was constructed in such a way that, in the (x,y) plan, the aircraft is always re-orienting horizontally to the HAC.
The angular misalignment between the direction vector to the target point (9) and the speed in the (x,y) plane is measured using the dot product. The direction is measured by the z component of the exterior product ($\wedge$) between the direction vector to the target point $\mathbf{P}_i$ and the aircraft speed $\mathbf{V}_i$. With $\mathbf{P}'_i = P_{i_x} e_x + P_{i_y} e_y$ and $\mathbf{V}'_i = V_{i_x} e_x + V_{i_y} e_y$, in order to align the aircraft to the target point in the (x,y) plane, the new bank angle is,

$$\begin{aligned} \mu_{i+1}^{hea} &= -T_{hard} \arccos \frac{\mathbf{P}'_i . \mathbf{V}'_i}{||\mathbf{P}_i|| \times ||\mathbf{V}_i||} \mathrm{Sign}((\mathbf{P}_i \wedge \mathbf{V}_i)_z) \\ &= -T_{hard} \arccos \left(\frac{P_{i_x} V_{i_x} + P_{i_y} V_{i_y}}{\sqrt{(P_{i_x}^2 + P_{i_y}^2)(V_{i_x}^2 + V_{i_y}^2)}} \right) \mathrm{Sign}\left[P_{i_x} V_{i_y} - P_{i_y} V_{i_x} \right] \end{aligned} \tag{11}$$

where, we have introduced a new constant $T_{hard} \in [0,1]$. The higher this constant, the faster the vehicle will turn for the same angular deviation.
We impose now a security threshold in the bank angle, μ_{max}. A typical value for the maximum bank angle is $\mu_{max} = \pm 70^o$. Therefore, the new control bank angle is,

$$\mu_{i+1} = \min\{|\mu_{i+1}^{hea}|, |\mu_{max}|\} . \mathrm{Sign}(\mu_{i+1}^{hea}) . \tag{12}$$

5 Simulations

In the previous section, we have described a control mechanism in order to guide a glider to a target. At each time step, the algorithm determines the shortest path to the target and determines the unique values of the attitude commands of the glider that are compatible with the aerodynamic characteristics of the glider. We now test this algorithm with some numerical simulations.

We have taken the glider initial coordinates $(x_0, y_0, z_0) = (0, 0, 40000)$ m, $V_0 =$ 1000 m/s, $\gamma_0 = 0$, $\chi_0 = 0$, $\mu_0 = 0^o$, $\alpha_0 = 30^o$, $T_{con} = 0.1$ and $T_{hard} = 1.0$, and we calculated the trajectories of the glider by numerically intreating equations (3) with a fourth order Runge-Kutta integration method.

The goal was to reach some target point that we have defined as the centre point of the HAC. We have chosen three different target HAC points with coordinates,

1) $(x_f, y_f, z_f) = (200\,000, 10\,000, 3\,000)$ m (figure 5).
2) $(x_f, y_f, z_f) = (50\,000, 10\,000, 3\,000)$ m (figure 6).
3) $(x_f, y_f, z_f) = (0, 10\,000, 3\,000)$ m (figure 7).

and we have calculated the controlled trajectories from the same initial point. The arrival to the HAC point occurs when the distance from the glider to the centre of the HAC point attains a minimum. This distance error will be denoted by e_d. In figures 5, 6 and 7, we show the glider controlled trajectories as function of time and

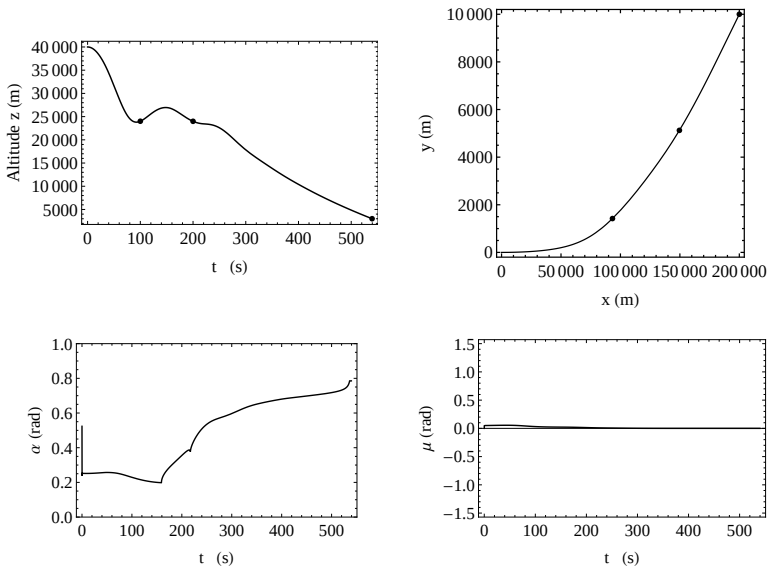

Fig. 5 Trajectory of the glider in the ambient space and control commands as a function of time. The coordinates of the HAC point target are $(x_f, y_f, z_f) = (200000, 10000, 3000)$ m. The time of arrival at the HAC is$t = 539.6$ s, with a distance error $e_d = 14.6$ m and final speed $V_f = 0.203$ M. The dots indicate the position of the glider after 100 s and 200 s of flight and the HAC position. Positive values of μ correspond to left turns and negative values of μ correspond to right turns.

the sequence of the attack and bank angle values as computed by the command and control algorithm. We have computed the time of arrival at the HAC, the final speed at the HAC (V_f) measured in Mach number units, and the distance error e_d.

The basic features of this algorithm is to guide the aircraft to the HAC point with very low distance errors. The choice of the initial conditions has been done insuring that the initial energy of the glider is enough to arrive at the target point. In this study, we have chosen target points within the maximum range calculated numerically by imposing the condition that the flight is always done with zero bank angle and maximum glide angle. In this case, the ratio C_L/C_D is maximal and the drag on the glider is minimal. For the initial conditions chosen and the Space Shuttle parameters, the range is of the order of 286 km.

Dynamic aircraft trajectories computed with the algorithm presented here depend on the control time T_{con}. For the conditions in figure 5, we have evaluated the distance error from the centre of the HAC as a function of T_{con}. For $T_{con} \leq 30$, we have found that,

$$e_d = 13.7 e^{0.049 T_{con}} . \tag{13}$$

In figure 8, we show the dependence of the distance error on the control time T_{con} for the initial and final conditions of the simulation in figure 5.

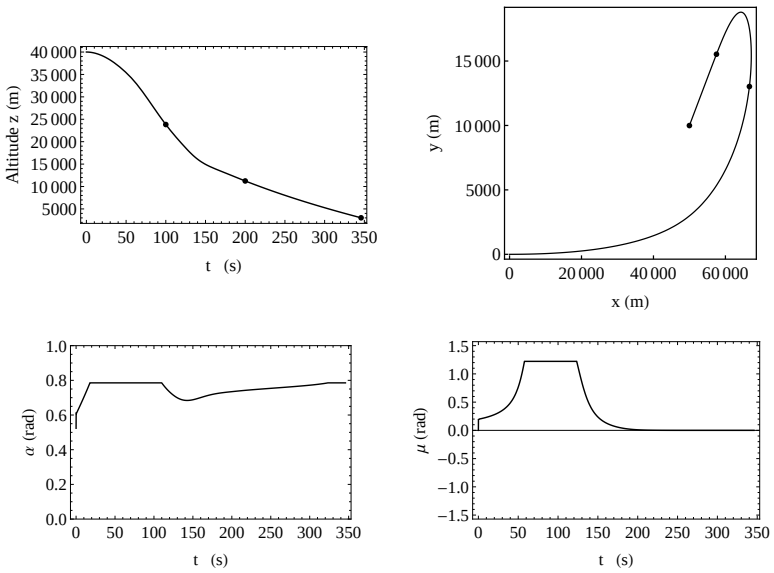

Fig. 6 Trajectory of the glider in the ambient space and control commands as a function of time. The coordinates of the HAC point target are $(x_f, y_f, z_f) = (50000, 10000, 3000)$ m. The time of arrival at the HAC is$t = 345.9$ s, with a distance error $e_d = 23.1$ m and final speed $V_f = 0.205$ M. The dots indicate the position of the glider after 100 s and 200 s of flight and the HAC position.

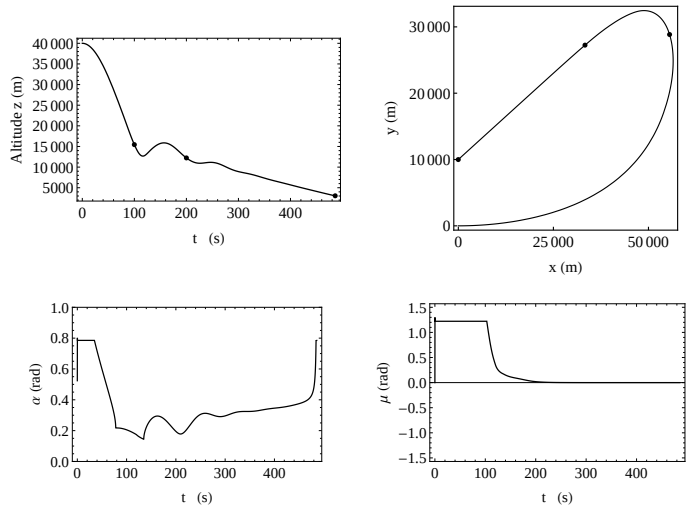

Fig. 7 Trajectory of the glider in the ambient space and control commands as a function of time. The coordinates of the HAC point target are $(x_f, y_f, z_f) = (0, 10000, 3000)$ m. The time of arrival at the HAC $t = 485.9$ s, with a distance error $e_d = 51.3$ m and final speed $V_f = 0.200$ M. The dots indicate the position of the glider after 100 s and 200 s of flight and the HAC position.

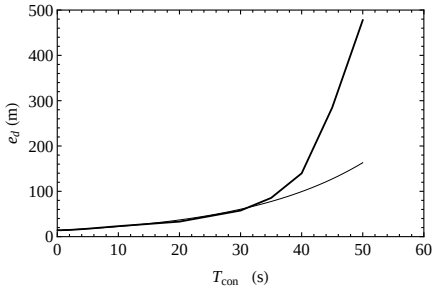

Fig. 8 Dependence of the distance error on the control time T_{con} for the initial and final conditions of the simulation in figure 5. For $T_{con} \leq 30$, the distance arrow follows the approximate exponential law (13), represented by the thin line.

We have also tested the dependence of the controlled trajectories as a function of the entry angle χ_0. In figure 9, we show the trajectories as in figure 5 but with $\chi_0 = \pi/4, 0, -\pi/4$. In this three cases, the distance errors are $e_d = 34.6$ m, $e_d = 14.6$ m and $e_d = 52.2$ m, respectively. For larger values of angles χ_0, the distance error can be as large as 69 km ($\chi_0 = \pi/2$).

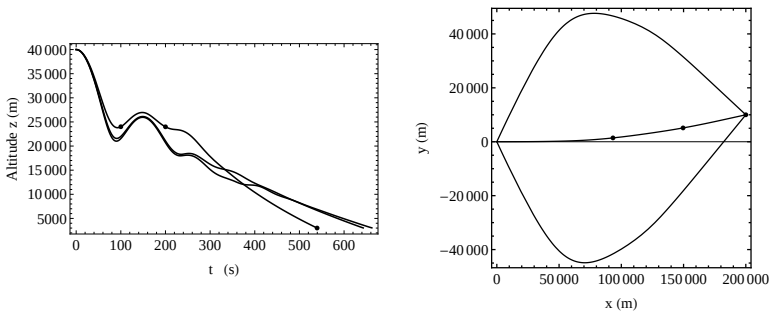

Fig. 9 Different trajectories calculated with the initial parameter $\chi_0 = \pi/4, 0, -\pi/4$. The other parameters are the same as in figure 5. For these trajectories, the distance errors are $e_d = 34.6$ m, $e_d = 14.6$ m and $e_d = 52.2$ m, respectively.

6 Conclusions

We have derived a new algorithm for the command and control during the TAEM phase of re-usable space vehicles. The algorithm determines locally the shortest path to the target point, compatible with the aerodynamic characteristics of the aircraft. We have tested the ability of the algorithm to guide the Space Shuttle during the

TAEM re-entry orbit, proving the feasibility of the algorithm, even using control times of the order of 30 s. Further refinements of the algorithm are under study [1].

Acknowledgements This work has been developed in the framework of a cooperation with AEVO GmbH (Munich) and we would like to acknowledge João Graciano for suggestions and critical reading of this paper. RD would like to thank IHÉS, where the final version of the paper has been prepared.

Appendix

The Earth atmosphere parameters are based on the 1976 US Standard Atmosphere Model. For the first seven layers we have used the formulas described in [10]. In table 2, we show the parameterisation of the thermodynamic quantities for the Earth atmosphere.

Layer	z_0 (m)	T_0 (K)	λ_0(K/m)	P_0 (Pa)
1	0	288.15	−0.0065	101325.00
2	11019	216.65	–	22632.10
3	20063	216.65	0.0010	5474.89
4	32162	228.65	0.0028	868.02
5	47359	270.65	–	110.91
6	51412	270.65	−0.0028	66.94
7	71802	214.65	−0.0020	3.96

Layer	T (K)	P (Pa)	ρ (kg/m^3)
1	$T_0+\lambda_0(z-z_0)$	$P_0(\frac{T_0}{T})^{g(z)M_{air}/(R\lambda_0)}$	$\frac{P}{TR_s}$
2	T_0	$P_0 e^{-g(z)M_{air}(z-z_0)/(RT)}$	$\frac{P}{TR_s}$
3	$T_0+\lambda_0(z-z_0)$	$P_0(\frac{T_0}{T})^{g(z)M_{air}/(R\lambda_0)}$	$\frac{P}{TR_s}$
4	$T_0+\lambda_0(z-z_0)$	$P_0(\frac{T_0}{T})^{g(z)M_{air}/(R\lambda_0)}$	$\frac{P}{TR_s}$
5	T_0	$P_0 e^{-gM_{air}(z-z_0)/(RT)}$	$\frac{P}{TR_s}$
6	$T_0+\lambda_0(z-z_0)$	$P_0(\frac{T_0}{T})^{g(z)M_{air}/(R\lambda_0)}$	$\frac{P}{TR_s}$
7	$T_0+\lambda_0(z-z_0)$	$P_0(\frac{T_0}{T})^{g(z)M_{air}/(R\lambda_0)}$	$\frac{P}{TR_s}$

Table 2 Characteristic parameters for the lower layers of the atmosphere. z_0 is the lower altitude of the layer, $R = 8.31432$ J/(mol kg) and $R_s = 287.04$ J/(kg K) are gas constants, $M_{air} = 0.0289644$ kg/mol, $g(z) = g_0(R_E/(R_E+z))^2$ is the gravity acceleration, $g_0 = 9.80665$ m/s^2 is the standard gravitational acceleration constant and $R_E = 6.371\times10^6$ m is the Earth mean radius.

References

1. Dilão, R., Fonseca, J.: Trajectory generation and dynamic control of unpowered vehicles during the TAEM phase, pre-print, 2013.
2. Gallais, P.: Atmospheric Re-Entry Vehicle Mechanics, Springer.
3. Hull, D.G.: Fundamentals of Airplane Flight Mechanics, Springer.
4. Jiang, Z., Ordonez, R.: Trajectory Generation on Approach and Landing for RLVs Using Motion Primitives and Neighboring Optimal Control, July 2007 - Proceedings of the 2007 American Control Conference.
5. Miele, A.: Flight Mechanics, Vol. I, Theory of Flight Paths,Addison-Wesley, Reading MA, 1962.
6. Ramsey, P.E.: Space Shuttle Aerodynamic Stability, Control Effectiveness and Drag Characteristics of a Shuttle Orbiter at Mac Numbers from 0.6 to 4.96, 1972 NASA/MSFC.
7. Raymer, D.P.: Aircraft Design: A Conceptual Approach, AIAA Education Series Fourth Edition.
8. Shevell, R.S.: Fundamentals of Flight, Prentice Hall 2nd Edition.
9. Trelat, E.: Optimal Control of a Space Shuttle and Numerical Simulations, Proceedings of the Fourth International Conference on Dynamical Systems and Differential Equations, Wilmington NC USA, May 2002.
10. US Standard Atmosphere, NASA-TM-X-74335, 1976 NASA National Aeronautics and Space Administration.
11. Vernis, P., Ferreira, E.: On-Board Trajectory Planner for the TAEM Guidance of a Winged-Body, EADS Space Transportation.